University of Baghdad
College of Engineering
JE
JOURNAL OF ENGINEERING

Journal of Engineering
journal homepage: www.joe.uobaghdad.edu.iq
Number 1 Volume 27 January 2021

Mechanical and Energy Engineering

Roughness Effect on Thermo-Elasto-Hydrodynamic Performance of a 170° -Arc Partial Journal Bearing

Souad Jabbar Shamal *
M.Sc.
Mechanical Engineering Department
University of Kufa, Al-Najaf, Iraq
Email: souadjabbar94@gmail.com

Luay Al-Anasri
Prof.
Mechanical Engineering Department
University of Kufa, Al-Najaf, Iraq
Email: luays.alansari@uokufa.edu.iq

Ahmed Alhusseny
Asst. Prof.
Mechanical Engineering Department
University of Kufa, Al-Najaf, Iraq
Email: ahmedn.alusseini@uokufa.edu.iq
Mechanical, Aerospace and Civil Engineering Department, University of Manchester, UK
Email: ahmed.alhusseny@manchester.ac.uk

Adel Gharib Nasser
Senior Lecturer.
Mechanical, Aerospace and Civil Engineering Department
University of Manchester, UK
Email: a.g.nasser@manchester.ac.uk

ABSTRACT

In the current analysis, the effects of circumferential scratches along the inner surface of a 170° -arc partial journal bearing has been numerically investigated. Their impact on the thermo-elasto-hydrodynamic performance characteristics, including maximum pressure, temperature, deformation, and stress, has been examined thoroughly. The ANSYS Fluent CFD commercial code was employed to tackle the iterative solution of flow and heat transfer patterns in the fluid film domain. They are then applied to the ANSYS Static Structure solver to compute the deformation and stress resulted in the solid bearing zone. A wide range of operating conditions has been considered, including the eccentricity ratio ($0.8236 \leq \varepsilon \leq 0.9866$) and scratch depth ($0mm \leq hs \leq 0.224mm$). In contrast, the bearing length-diameter ratio (L/D) and the rotation speed (N) have been fixed at 0.77 and 1500 rpm, respectively. The thermo-hydrodynamic pressure, temperature, stress, and deformation have all been computed. It was found that the scratch depth has a direct effect on the thermo-hydrodynamic performance of the partial bearings. Meanwhile, the deep central scratches are important, especially at scratch depth equal to 0.224mm.

Keywords: Partial Journal Bearings, Surface Roughness, CFD Analysis, Fluid-Solid Interaction(FSI) Analysis, Thermo-elasto-hydrodynamic Performance.

*Corresponding author
Peer review under the responsibility of University of Baghdad.
https://doi.org/10.31026/j.eng.2021.01.02

Article received: 19/7/2020
Article accepted: 14/9/2020
Article published:1/1/2021

تأثير الخشونة على الأداء الحراري- المرن- الهيدروديناميكي لمحمل جزئي بقوس 170 درجة

سعاد جبار شمال*
طالبة ماجستير
كلية الهندسة- جامعة الكوفة

لؤي الانصاري
استاذ
كلية الهندسة- جامعة الكوفة

احمد الحسيني
استاذ مساعد
كلية الهندسة- جامعة الكوفة
كلية الهندسة- جامعة مانشستر

عادل غريب ناصر
مدرس اقدم
كلية الهندسة- جامعة مانشستر

الخلاصة

في الدراسة الحالية، تم دراسة تأثير الخدوش المحيطية المتولدة على السطح الداخلي لمحمل جزئي بقوس 170 بشكل عددي. تم اختبار تأثير تلك الخدوش على خصائص الأداء الحراري-المرن-الهيدروديناميكي مثل الضغط الأقصى المتولد، درجة الحرارة، التشوه والاجهاد. تم استخدام برنامج ANSYS Fluent لتنفيذ الحل العددي والتكراري لمجال الجريان وانتقال الحرارة في منطقة زيت التشحيم، ومن ثم تم تطبيق كل من الضغط والحمل الحراري المتولدين على السطح الداخلي للمحمل كشروط حدية لبرنامج ANSYS Static Structural لأجل التنبؤ بالتشوه والاجهاد الناتجين في منطقة المحمل الصلبة. تم النظر في مجموعة واسعة من ظروف التشغيل بما في ذلك نسبة الانحراف $(0.8236 \leq \varepsilon \leq 0.9866)$ وكذلك عمق الخدش $(0mm \leq hs \leq 0.224mm)$، بينما تم تثبيت كل من نسبة طول إلى قطر المحمل (L/D) وسرعة الدوران (N) عند كل 0.77 و 1500 rpm، على التوالي. تم احتساب توزيع كل من ضغط الزيت ودرجة الحرارة لكل من الزيت والمحمل اضافة الى كل من التشوه والاجهاد المتولدين عبر المحمل الصلب. لقد وجد أن عمق الخدش له تأثير مباشر على الأداء الحراري-المرن-الهيدروديناميكي للمحامل الجزئية. كذلك، يبدو أن الخدوش المركزية الأكثر عمقاً لها تؤدي الى تأثيرات بالغة على أداء المحمل خصوصاً عندما يكون عمق الخدوش مساوٍ للخلوص المحيطي للمحمل، أي (0.224mm) ملم.

الكلمات الرئيسية: المحامل الجزئية ، خشونة السطح ، تحليل CFD ، تحليل تداخل المائع- الصلب(FSI), الأداء الحراري المرن الهيدروديناميكي.

1. INTRODUCTION

Partial journal bearing is one of the most common applications of tribology. It is widely used in industrial and daily life applications, including rotary kilns, cement mills, and many other rotating machineries. It consists of three main parts; the fixed part (bearing), running part (journal), and fluid layer (lubricant) between the two parts(bearing and journal). The lubricant is used to reduce wear, friction, and temperature generated due to friction, as shown in **Fig. 1**.

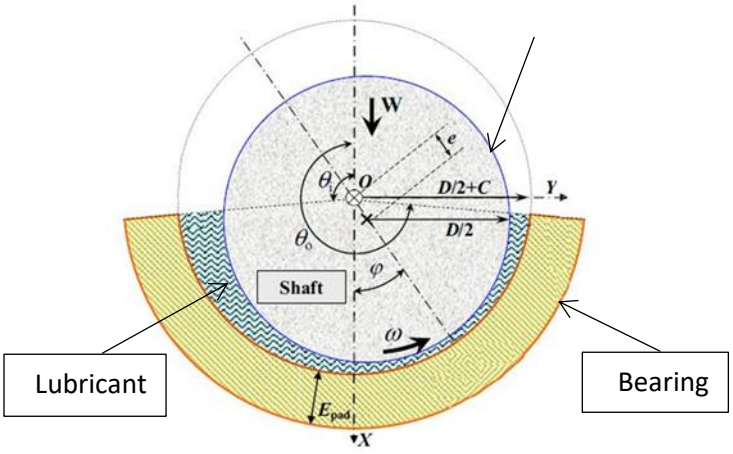

Figure 1. The geometrical shape of partial journal bearing **(Dobrica and Fillon,2012).**

Surface roughness can be defined as a component of surface texture. It is usually measured by the surface deviations formed perpendicularly compared to its ideal form. If such deviations are considerable, the surface is said to be rough; otherwise, it is considered smooth if it includes small

deviations. The roughness of an engineered surface may be classified as: a random roughness resulting from surface finishing or a deterministic roughness planned intentionally to increase the lubrication characteristics of the hydro-dynamically lubricated thrust ring**(Vyas, 2005)**. A very general classification for a solid surface is shown in **Fig. 2**.

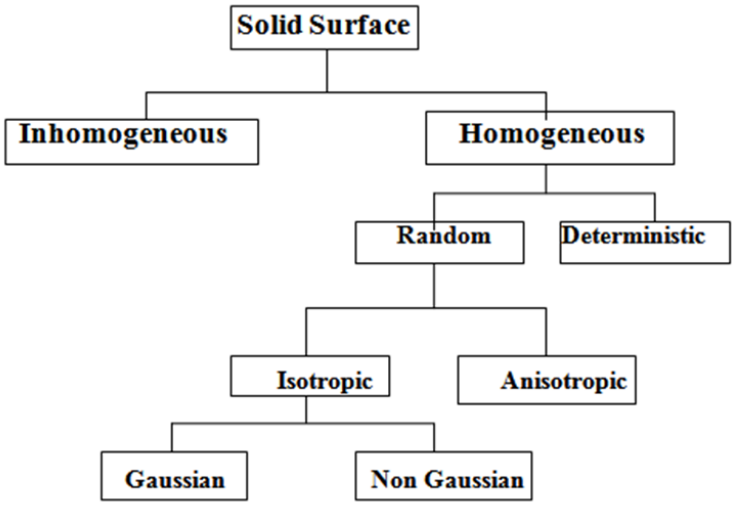

Figure 2. The general classification of a solid surface **(Vyas, 2005).**

(Sharma and Pandey, 2005) have analyzed the influence of longitudinal surface roughness on thermo-hydrodynamic lubrication. An infinitely wide plane slider bearing has been investigated numerically using a stochastic roughness model. As the height of surface roughness increases, it showed that the value of film-thickness ratio "at which maximum load-carrying capacity (isothermal) has been recorded" decreases. In contrast, a significant reduction in load-carrying capacity (thermal) has been recorded with the lubricant temperature rise due to the roughness parameter increase.

(Dobrica et al., 2006) examined a specific numerical model viable on partial journal bearing operating in mixed lubrication region. Simulations have been done for various models of roughness and eccentric ratio (0.8-1.08). It was apparent that surface roughness affected all performance characteristics of bearing, including fluid film thickness, angle of attitude, and friction- torque. However, the roughness effect seems to have largely depending on the direction of roughness. Compared to smooth surfaces and by used hypothesis rigid pad (HD) model, it showed the largest effect of roughness resulting in an increase of (30%) in the minimum mean film–thickness and more of (54%) in friction torque. The roughness of isotropic properties had a smaller effect but still had a large impact on bearing performance. On the other hand, the longitudinal -roughness seemed had an effect only on friction- torque. When the deformation is allowed in pad response to the hydrodynamic- pressure model, it was observed that the overall effect of roughness is greatly diminished.

The elasto-hydrodynamic lubricant analysis (EHL) for a 60º radial partial bearing is analyzed by (**Bhat et al., 2007**) using the CFD (Computing-Fluid-Dynamics) with CSD (Computing-Structural- Dynamics). This combined field analysis employs the calibers of the ANSYS / FLOTRAN commercially available finite element program with fluid-solid interaction (FSI) technology. The pressure is found by using computational fluid dynamics, considering that the

flow is laminar. The distribution of deformations and stresses on the bush is obtained due to the pressure of pressure using the finite element method satisfying the boundary conditions.

The circumferential scratches which appear in the inner bearing surface were studied analytically by **(Dobrica and Fillon, 2008)** and explained their effect on the thermo-hydrodynamic performance- characteristics such as minimum film thickness (h_{min}), the maximum pressure (P_{max}), mean oil film temperature (T_{mean}), and friction torque. The effects predicted were especially important for central-deep scratches. It seems that the most important parameter for measuring the intensity of scratching is the worn-out area. When the scratches spread over the inner bearing surface, they are likely to lead to the bearing's destruction, even if it is comparatively slim and represents a small section from the total bearing width. The other important parameter is the depth of the scratch, as deep scratches were found to reduce the local pressure about to surrounding pressure. It was also noticed that the density of scratch appears to be only important for scratches surface [$h_s < C/4$], or when a few areas of bearing is destruction. Finally, smaller wear impacts are found when scratches are moved toward the bearings edges.

(Dobrica et al., 2008) presented developed deterministic partial elasto- hydrodynamic journal bearing play in the mixed-lubrication system by taking the rough surface into account. Reynolds' equation was solved on a very thin grid, and the pad deformation resulting from isothermal-pressure was taken into consideration. The results appeared the partial bearing's geometry and the shaft speed equal to 0.47 m / sec, at specific- pressure value ranging up to 50 MPs. The pad materials were taken into account for both iso-viscous and piezo-viscous oil lubricant. The simulation results were demonstrated in terms of specific pressure, relative eccentricity ratio, oil film thickness, contact extent, friction torques, etc. Surface roughness has been shown to have a large effect on the performance of bearing, mainly when the loads are high where the rough contact amount is available and large. The longitudinal- roughness trends appear weaker behavior, whereas transverse- roughness trends appear better overall performance.

(**Abass et al., 2010**) have examined partial journal bearings' performance based on a steady-state thermo-hydrodynamic model (THD) for partial journal bearings. The generalized Reynold's - equation, the energy equation in oil- film, and the equation of heat transfer in pad and shaft are solved simultaneously. The shaft temperature has been found a large influence on the bearing performance, where both oil and bush temperature increase, with the rise in shaft temperature while the oil film thickness decreases.

Isothermal hydrodynamic analysis was conducted numerically by **(Dobrica and Fillon, 2012)** to evaluate the scratched journal bearings' overall performance degradation. The scratches' severity was measured by using four parameters, namely the scratch depth, the scratched extent area, the scratches density, and the scratched location. To evaluate overall bearing performance degradation, several working parameters were calculated minimum oil film thickness (h_{min}), mean oil temperature (T_{mean}) and maximum hydrodynamic pressure (P_{max}). Most of the examined parameters seem to have a direct impact on bearing performance, where it was found that the numerous/denser/deeper the scratches, the poorer the bearing performance. In general, the scratch depth seems to be the most dominant parameter, where if it is relatively small compared to film thickness, the bearing performance is slightly affected. Otherwise, the performance is severely affected when the scratches are getting deeper, which means that the deterioration in performance can be minimal in a low-load bearing and adverse in a high-load bearing, which similarly complicates the contrast from scratch effects.

(Liang et al.,2016) investigated the hydrodynamic -performance of lubrication, a partial textured-sliding journal bearing utilizing the CFD ADINA program. The limit requirement of the phase change has been applied to the fluid field. It was found that texture found at the lubricant entrance

area that the bearing performance can improve. Otherwise, bearing performance is reduced because of the texture found in the area of maximum pressure. While the texture found at the outlet region of lubricant has two various consequences: a portion of the texture found inside the divergent area of oil film improves the load-carrying capacity, but the portion outside the divergent area makes the load-carrying capacity decrease.

In the current research, the effects of circumferential scratches along the inner surface of a 170^{o} - arc partial journal bearing has been numerically studied. Based on an FSI analysis, the impact of scratches on the thermo-elasto-hydrodynamic performance characteristics, including maximum pressure, temperature, deformation, and stress, has been examined thoroughly and various design and operating conditions.

2. MATHEMATICAL Model

The mathematical model in this study is divided into two parts. The first is the fluid film layer (lubricant), while the other is the solid structural (bearing or pad), as previously shown in **Fig.1**. In this study, the bearing (bush) 's inner surface is scratched circumferentially along the pad length, as shown in **Fig.3**, where the bearing is assumed to be made of brass alloy.

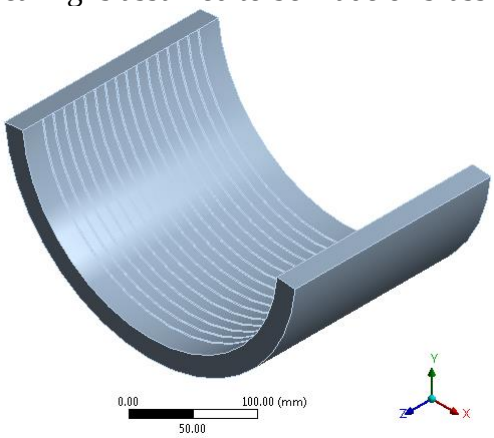

Figure 3. Scratched bearing bush by Ansys workbench (17.2).

The governing equations used along with the appropriate boundary conditions required to close a mathematical model will be detailed for both the fluid film zone (lubricant) and solid zone (bearing), as follows:

2.1. Governing equations of fluid film zone (lubricant)

The partial differential equations governing the conservation of mass and momentum (Navier-Stokes equations) for the fluid film layer are as follows **(Versteeg and Malalasekera, 2007)**:

$$\frac{\partial u}{\partial x}+\frac{\partial v}{\partial y}+\frac{\partial w}{\partial z}=0 \tag{1}$$

$$\rho_f\left(u\frac{\partial u}{\partial x}+v\frac{\partial u}{\partial y}+w\frac{\partial u}{\partial z}\right)=-\frac{\partial p}{\partial x}+\mu\left(\frac{\partial^2 u}{\partial x^2}+\frac{\partial^2 u}{\partial y^2}+\frac{\partial^2 u}{\partial z^2}\right) \tag{2}$$

$$\rho_f\left(u\frac{\partial v}{\partial x}+v\frac{\partial v}{\partial y}+w\frac{\partial v}{\partial z}\right)=-\frac{\partial p}{\partial y}+\mu\left(\frac{\partial^2 v}{\partial x^2}+\frac{\partial^2 v}{\partial y^2}+\frac{\partial^2 v}{\partial z^2}\right) \tag{3}$$

$$\rho_f\left(u\frac{\partial w}{\partial x}+v\frac{\partial w}{\partial y}+w\frac{\partial w}{\partial z}\right)=-\frac{\partial p}{\partial z}+\mu\left(\frac{\partial^2 w}{\partial x^2}+\frac{\partial^2 w}{\partial y^2}+\frac{\partial^2 w}{\partial z^2}\right) \tag{4}$$

Where ρ_f, p, u, v, w stand for the lubricant density, pressure, x, y, and z- velocity component, respectively. μ stands for the dynamic lubricant viscosity, and it is assumed to vary exponentially with lubricant temperature as:

$$\mu = \mu_i e^{-\beta(T_f - T_i)} \quad (5)$$

Where μ_i is the dynamic viscosity of the lubricant at the inlet temperature T_i, while β represents the temperature-viscosity coefficient of the lubricant.

Besides the Navier-Stokes equations, the fluid- energy equation should be solved to find the temperature distribution of the film layer is as follows **(Versteeg and Malalasekera, 2007)**:

$$\frac{\partial(\rho_f c_\rho T_f)}{\partial t} + div\left(\rho_f c_\rho T_f \mathrm{u}\right) = -p div\ \mathrm{u} + div\left(\lambda_f\ grad\ T_f\right) + S_T \quad (6)$$

Where c_ρ, λ_f , T_f are respectively the lubricant specific heat, lubricant thermal conductivity, and lubricant temperature, while S_T represents a source term.

2.2. Boundary conditions for fluid film zone (lubricant)

2.2.1. Hydrodynamic boundary conditions

As solid walls surround the film flow, no-slip occurs on each journal and bearing surfaces. This implies that the lubricant particles in the rotating journal's vicinity always have zero velocity relative to the rotating shaft to maintain the non-slip condition. Moreover, the condition at the sidewalls bounding the film field is assumed to be at an atmospheric state, i.e. zero gauge pressure. Thus, the boundary conditions used are as shown in **Fig.4**:

A-At the journal bearing edges; $z = \mp\frac{L}{2}$, $p = p_{atm} = 0$

B-At the inner surface of fluid film; $r = R_j$, $u_\theta = \omega R_j$, $u_r = u_z = 0$

C-At the outer surface of fluid film; $r = R_{bi}$, $u_\theta = u_r = u_z = 0$ (7)

2.2.2. Thermal boundary conditions

The distribution of temperatures through the fluid film thickness can be found by solving the equation of energy and through using the following boundary conditions:

2.2.2.1. Inlet boundary

It is assumed that a γ fraction of the lubricant leaving the system is recirculated and mixed with a fresh amount of lubricant at colder condition, i.e., T_0 =40°C, to maintain the working lubricant at acceptable operating conditions. Thus, the lubricant film temperature at the inlet section as:

$$T_{in} = \frac{[Q_{lateral1} + Q_{lateral2} + (1-\gamma)Q_{out}]T_o + \gamma Q_{out} T_{out}}{Q_{in}} \quad (8)$$

Where Q stands for the lubricant volume flow rate across any of the non-solid boundaries enclosing the film layer.

2.1.1.1 Outlet boundary

According to the formulation developed by **(Khonsari and Booser, 2006)**, the shaft temperature can be estimated as:

$$T_{shaft} = \frac{\bar{T}_{shaft}}{\beta} + T_i \quad (9)$$

Where $\bar{\bar{T}}_{shaft}$ stands for the dimensionless shaft temperature and can be computed as:

$$\bar{T}_{shaft} = \left(a + \frac{b}{K_1^{0.5} K_1^{0.5}} + \frac{c}{K_2^2 K_2^2}\right)^{-1} \quad (10)$$

Where K_1 and K_2 are coefficients used to predict the journal surface temperature defined as:

$$K_1 = \frac{\alpha_0 \mu_i \beta U}{\lambda_f R_j} \left(\frac{R_j}{C}\right)^2 \quad (10.a)$$

$$K_2 = U\sqrt{\mu_i \beta / \lambda_f} \quad (10.b)$$

Where:

$0.001 \leq K_1 \leq 0.5$ and $0.01 \leq K_2 \leq 5$

and $\alpha_o = \lambda / \rho_f c_p$ is the lubricant thermal diffusivity, while a, b, c are constants depending on and α_o:

$$\left.\begin{array}{llll} 0.1 < \varepsilon < 0.3: & \text{a} = 0.14092, & \text{b} = 0.24303, & \text{c} = 0.10054 \\ 0.3 \leq \varepsilon \leq 0.7: & \text{a} = 0.04734, & \text{b} = 0.39751, & \text{c} = 0.11007 \\ 0.7 < \varepsilon \leq 0.9: & \text{a} = 0.06200, & \text{b} = 0.38364, & \text{c} = 0.10102 \end{array}\right\} \quad (11)$$

2.2.2.3. Side Surface of Film Layer

Due to a negligibly thin layer of lubricant exposed to the ambient, the side surfaces of the lubricant can be assumed thermally insulated as:

$$\frac{\partial T_f}{\partial z} = 0 \quad (12)$$

2.2.2.4. The Lubricant-Bearing Interface

The solution of temperature field in the solid bearing zone is linked to the temperature distribution in the fluid film through the surface of the interface between the two zones as follows:

$$-\lambda_s \left.\frac{\partial T_s}{\partial x_n}\right|_{bi} = h_{bi}\left(T_{bi} - T_{film\_b}\right) \quad (13)$$

Where the temperature and heat transfer coefficient on the inner bearing surface T_{bi}& h_{bi}, are implicitly computed from the conjugate heat transfer rate between the fluid film field and the solid bearing zone.

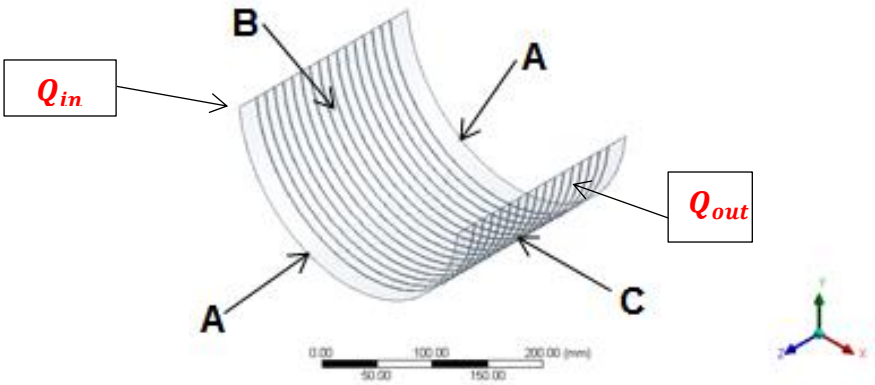

Figure 4. Boundary conditions for fluid film.

2.3. Governing equations of the **solid zone (bearing)**

For the solid domain, the partial differential equations governing can be described using the second law of motion **(Liu *et al.* , 2010)**:

$$\rho_s \ddot{\delta} = \nabla . \sigma_s + f_s \quad (14)$$

2.4. Hydrodynamic boundary conditions of the solid zone (bearing)

The solid bearing is exposed to an internal pressure load resulting from the lubricant flow field, while the external wall is considered to be fixed. Furthermore, the side boundaries are maintained free-loaded. Thus, the boundary conditions used are as shown in **Fig. 5**:

$$\left.\begin{array}{ll} \textbf{D}\text{-At the journal bearing edges;} & z = \pm\frac{L}{2} \quad \rightarrow F = 0 \\ \textbf{E}\text{-At the inner surface of bearing;} & r = R_{bi} \quad \rightarrow F = \mathrm{p}(\theta, z)dA \\ \textbf{F}\text{-At the outer surface of bearing;} & r = R_{bo} \quad \rightarrow \delta = 0 \end{array}\right\} \quad (15)$$

2.5. Thermodynamic boundary conditions of the solid zone (bearing)

The thermal conditions that are required to bound the solid energy equation are divided into two types according to the region where they are applied to. The first type is the one that is applied over the inner surface of the bearing, which has already been stated before, i. e. **Eq. 13**. The other sort is applied over the outer and side surfaces of the bearing, which are subjected to free convection heat transfer as:

$$-\lambda \frac{\partial T_b}{\partial x_n}|_{bo} = h_{bo}(T_{bo} - T_a) \quad (16)$$

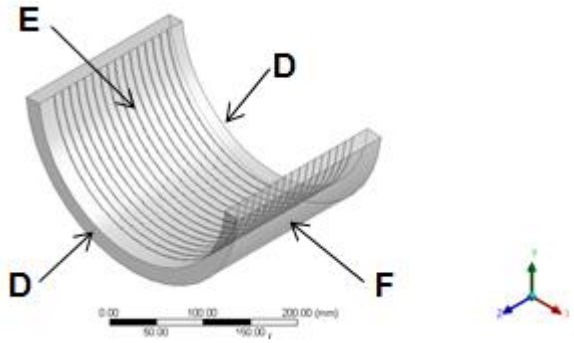

Figure 5. Boundary conditions for the solid domain(b earing).

3. NUMERICAL ANALYSIS

The partitioned one-way coupling is employed in the fluid-solid interaction present. The fluid film pressure is first computed using the well-known ANSYS Fluent CFD commercial code. It is then transferred to the ANSYS Static Structure solid solver to compute the deformation and stress resulting in the solid bearing zone. Both fluid film and solid bearing zones have been discretized into a number of hexahedral elements, as shown in **Fig. 6**. The solution method used for CFD simulation is based on the second-order upwind differencing scheme. The discretized equations for the lubricant flow field have been solved iteratively according to the SIMPLE algorithm **(Versteeg and Malalasekera, 2007)**. A user-defined UDF code has been written and compiled into ANSYS Fluent solver to compute the temperature-dependent lubricant viscosity, **Eq. 5**, and determine the lubricant temperature at the inlet boundary, **Eq. 8**, as well as the shaft surface, **Eq.9**. The grid dependency was checked for three sets of the film and solid mesh to examine the sensitivity of the results computed to the number of grid divisions along each of the physical coordinates, i.e., radial ni, circumferential nj, and axial n_k. In general, it has been observed that the number of divisions along the radial direction ni dominates the accuracy of the solution obtained, unlike the number of divisions along with the other two directions, i.e., nj or n_k, which have no noticeable impact, as shown in **Table 1**. A mesh grid size of (ni =2, nj =400, n_k =600) is considered for fluid flow zone. The maximum aspect ratio ranges from 9 to 57, minimum orthogonal quality ranges from 0.68 to 0.99, and maximum ortho-skew ranges from 0.0003 to 0.2.

For the bearing zone, a grid size of (ni =10, nj =400, n_k =600) is considered, the aspect ratio equals 1.20 with minimum orthogonal of 0.999 and maximum ortho-skew of 4.44*10-3. Accordingly, for all the simulations to be carried out, the selected grid dimensions result in a reasonable mesh quality in the current investigation.

Table 1. Grid Dependence at ε=0.82, L/D=0.77, N=1500r.p.m and θ=170 Deg.

n_i	n_j	n_k	Number of Element($n_i \times n_j \times n_k$)	Max. Pressure(Pas)
2	400	600	480000	11700000
3	400	600	720000	14500000
4	400	600	960000	15800000
5	400	600	1200000	16400000
6	400	600	1440000	16800000
7	400	600	1680000	17700000
8	400	600	1920000	17500000
9	400	600	2160000	18100000
10	400	600	2400000	18100000

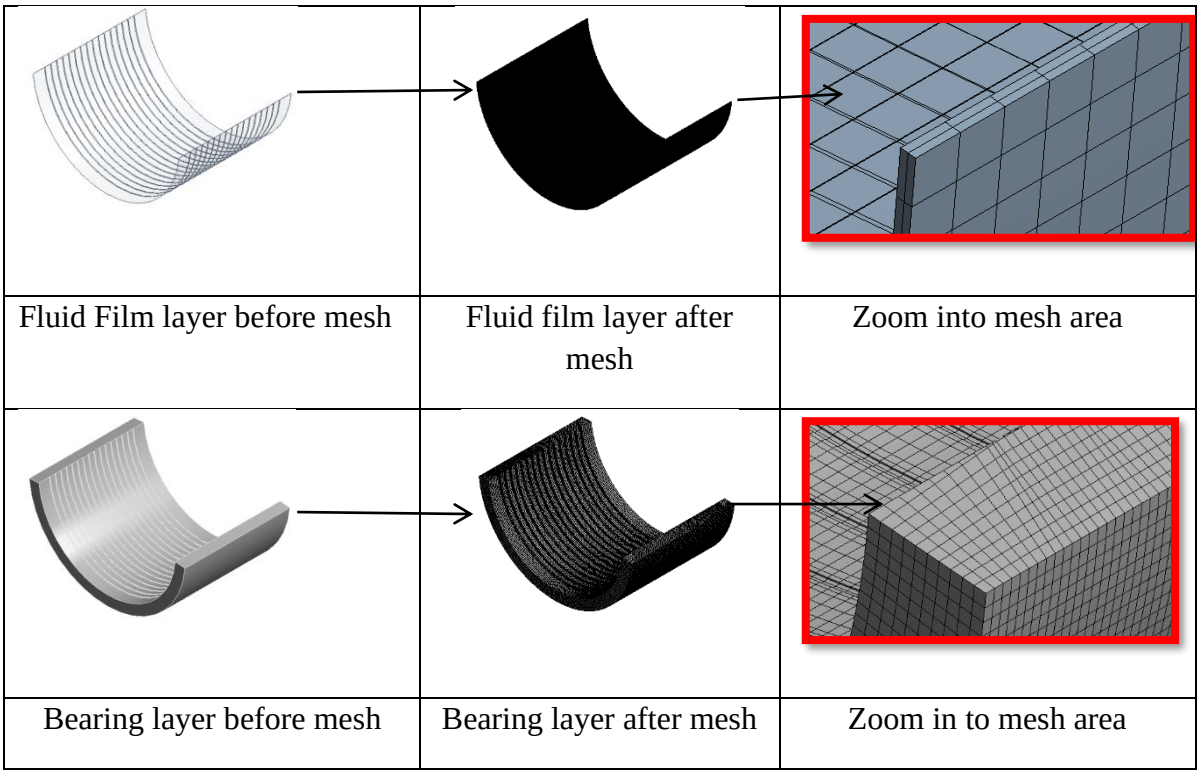

Figure 6. Mesh generated for fluid film and bearing zones using hexahedral cells.

Under-relaxation factors are applied to the solution of the lubricant flow domain to overcome potential instability during the iterative solution, as shown in **Fig.7**.

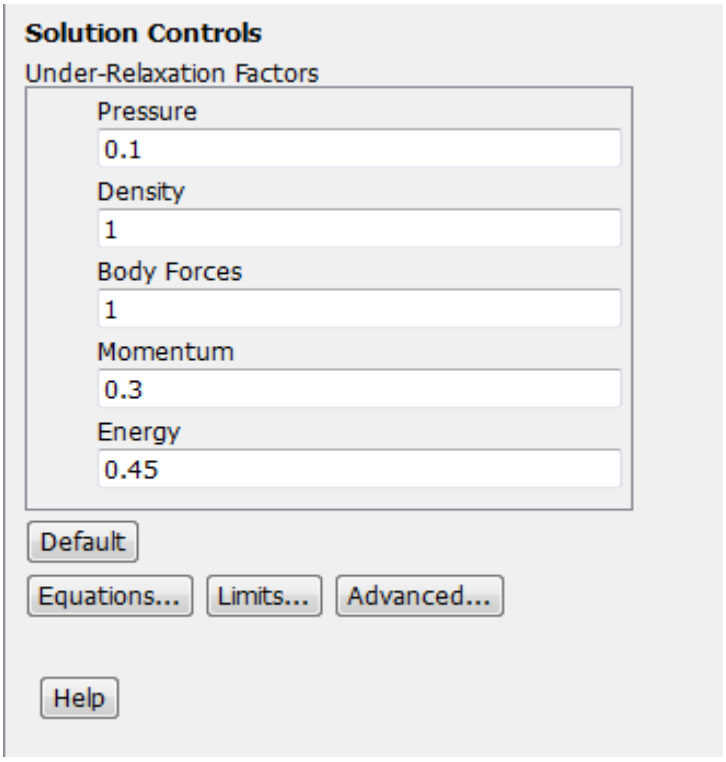

Figure 7. Under relaxation factors (URF) used in the present study.

Due to the lack of research presented in the field of scratched partial journal bearings, the methodology adopted in the present work has been validated against the numerical data computed by **(Dobrica and Fillon, 2012)** regarding the thermo-hydrodynamic performance of a scratched partial journal bearing. The focus is to inspect the hydrodynamic and thermal patterns while operation for five journal bearings of different scratch depth (h_s=0, *C*/8, *C*/4, *C*/2, and *C*), as in **Fig. 8**, where the design parameters regarding the cases tested are detailed in **Table 2**. The length–diameter ratio (L/D) equals (0.77) and the clearance –radius – ratio (C/R) equals (0.0016). The journal operates at 1500 rpm, and the ISO VG 32 oil is supplied at 40°C. A global thermal model is used to account for oil heating due to viscous effects. It is supposed that 30% of the oil is supplied at 40°C, and 70% of the flow is recirculating. The oil used density is set to 860 kg/m^3 and its dynamic viscosity to 0.03 Pa.s. The pressure profile variation along the journal pad is generally in agreement with that presented by **(Dobrica and Fillon, 2012)**. However, there is a significant mismatch in the values of maximum pressure computed, especially in the cases where deep scratches have been applied, i.e. $h_s \geq C/2$. This is attributed to the fact that the model solved by **(Dobrica and Fillon, 2012)** is not complete and includes many approximations that may have led to serious overestimations in the pressure produced. Due to the 2-dimensionality of the model adopted, no considerations have been given to the thermal conditions at the bush and journal surfaces, where 15% of the heat generated due to friction was assumed to be dissipated by the bush and journal surfaces, while the rest to be carried away by the lubricant. On the other hand, the current simulation considers more advanced procedures. A three-dimensional solution has been conducted based on more realistic boundary conditions applied, whether on the bush and journal surfaces or at the inlet and outlet sections of the bearing.

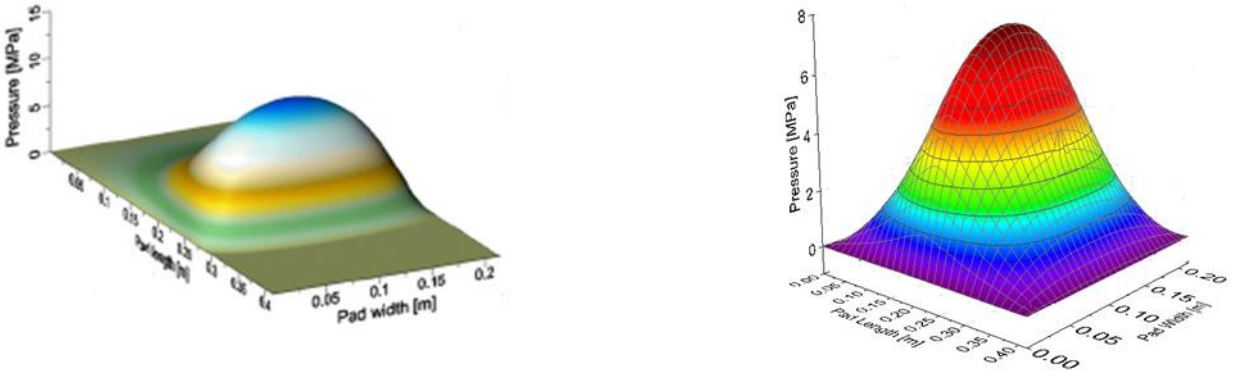

(a) $h_s = 0$

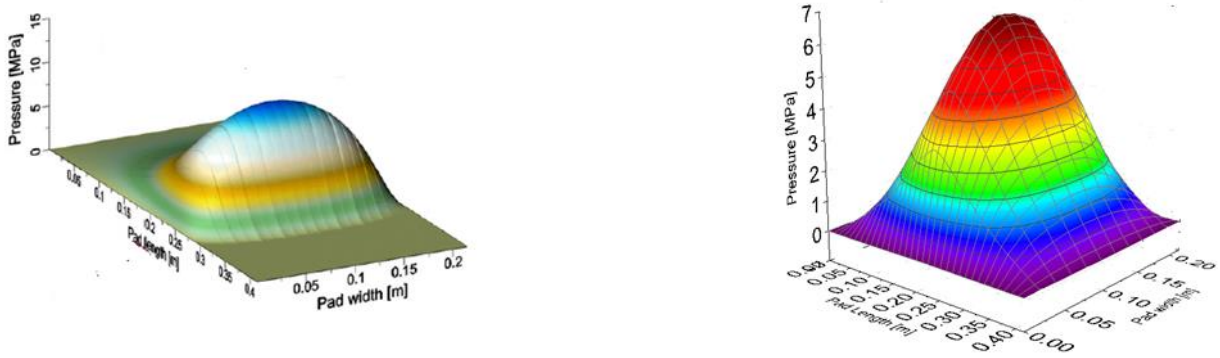

(b) $h_s = C/8$

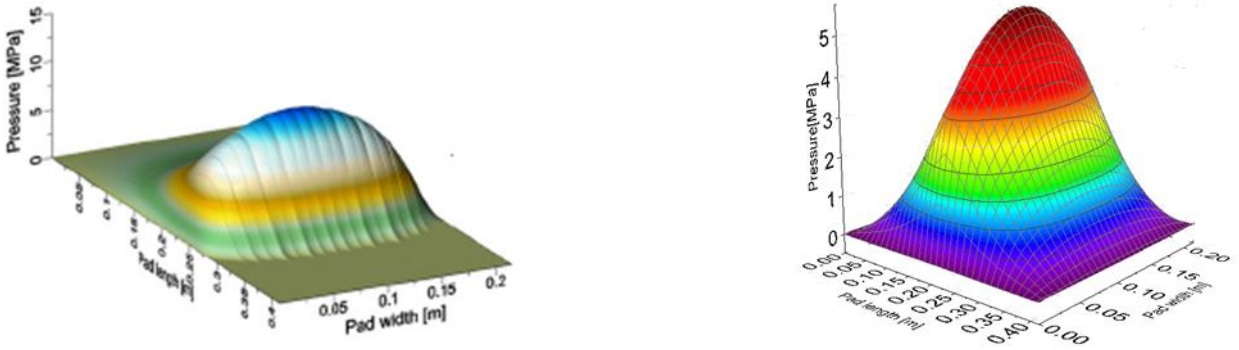

(c) $h_s = C/4$

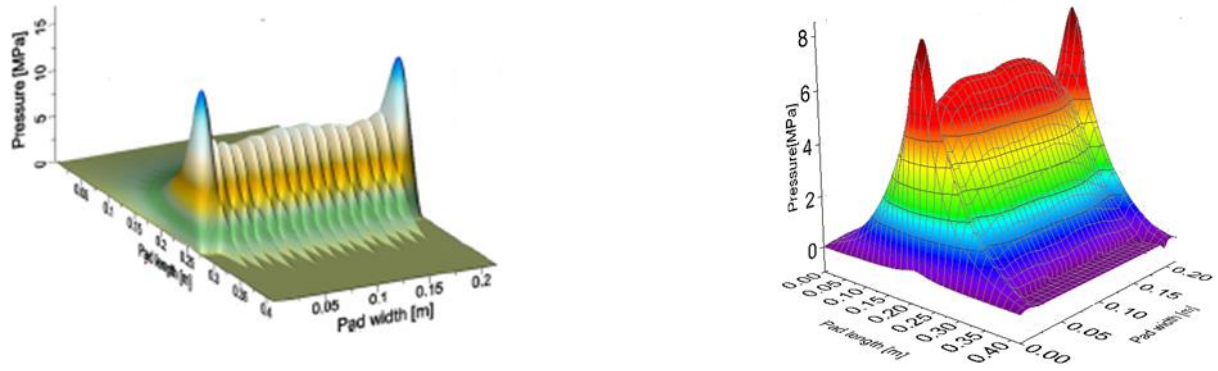

(d) $h_s = C/2$

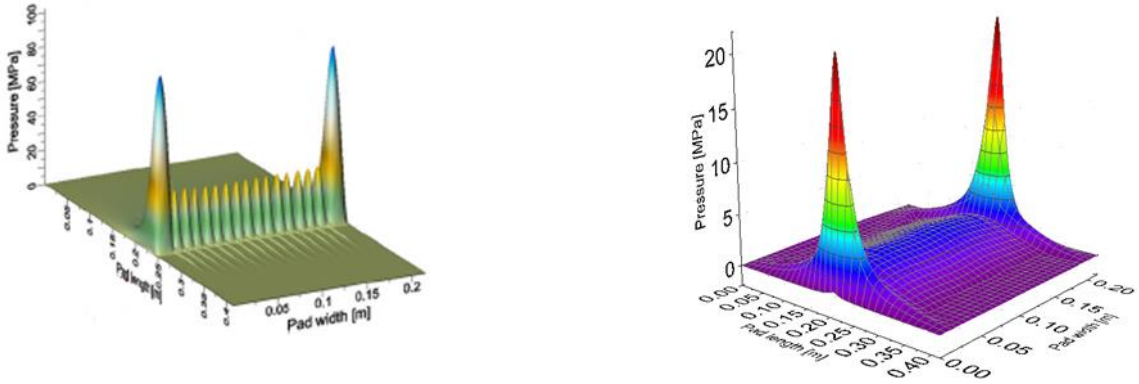

(e) $h_s = C$

Figure 8. A Comparison between the thermo-hydrodynamic pressure distribution obtained in the present work numerically (right) with the corresponding data measured numerically by (**Dobrica and Fillon**, **2012**).

4. RESULTS AND DISCUSSION

The effect of the circumferential scratches spread on the entire bearing surface, even if they are relatively thin and only represent a small amount of the total bearing width, which may lead to the destruction of the bearing. The dimensions of scratched partial journal bearing considered in the current analysis are detailed in **Table 2**.

Table 2. Partial journal bearing dimensions, **Dobrica and Fillon,2012.**

Parameter	Symbol	Data Setting and Unit
Shaft (Journal) radius	R_j	0.140 (m)
Radial clearance	C	0.000224 (m)
Inner bearing radius	R_{bi}	0.140224 (m)

External bearing radius	R_{bo}	0.160224 (m)
Bearing thickness	t	0.02 (m)
Leading edge position	θ_i	95 (Deg.)
Trailing edge position	θ_o	265 (Deg.)
Attitude angle	φ	0 (Deg.)
Bearing length	L	0.215 (m)
Eccentricity ratio	ε	0.82,0.836,0.8589,0.9616,0.9866
Number of scratches	N_s	16 (scratch)
Width of each scratch	W_s	0.001375 (m)
Depth of scratch	h_s	0.000028,0.000056,0.000112,0.224 (m)
Rotation speed	N	1500(r. p. m)
Bush convection heat transfer coefficient	$hconv$	80 ($W/m^2.^o C$)
Bush thermal expansion coefficient	α_b	19*10^-6 (C^{-1})
Modules of elasticity	E	127(GPa)
Poisson's ratio	ν	0.32
Tensile yield strength of baring	σ_Y	280(MPa)
The density of bearing material	ρ_b	8670 (Kg/m^3)

In light of these results, scratch depth is actually shown as the main parameter governing scratch effects: in the case of a smooth surface ($h_s = 0C$) In other words, no scratches on the entire bearing surface, where the maximum pressure developed in fluid film thickness, is shown in **Fig.9(a)**. Surface scratches (h_s=0.125 C) and (h_s=0.25 C)have almost no large effect on bearing performance, as in **Fig .9(b, c)**. As the scratch depth equals half value from radial clearance (h_s=0.5 C) have destructive effects, as shown in **Fig.9(d)**. At last, the deeper scratch equal to radial clearance (h_s= C) the pressure distribution on the bearing surface has been severely affected, where extremely high-pressure levels are generated, as shown in **Fig.9(e)**. This is due to the increased flow of oil in the scratch areas, which has a cooling effect. In fact, at the same deflection (and hence the same minimum film thickness), the scratched bearing will generate a much higher oil flow rate than the non-worn bearing, thus operating at a lower temperature (but also providing a lower bearing capacity).

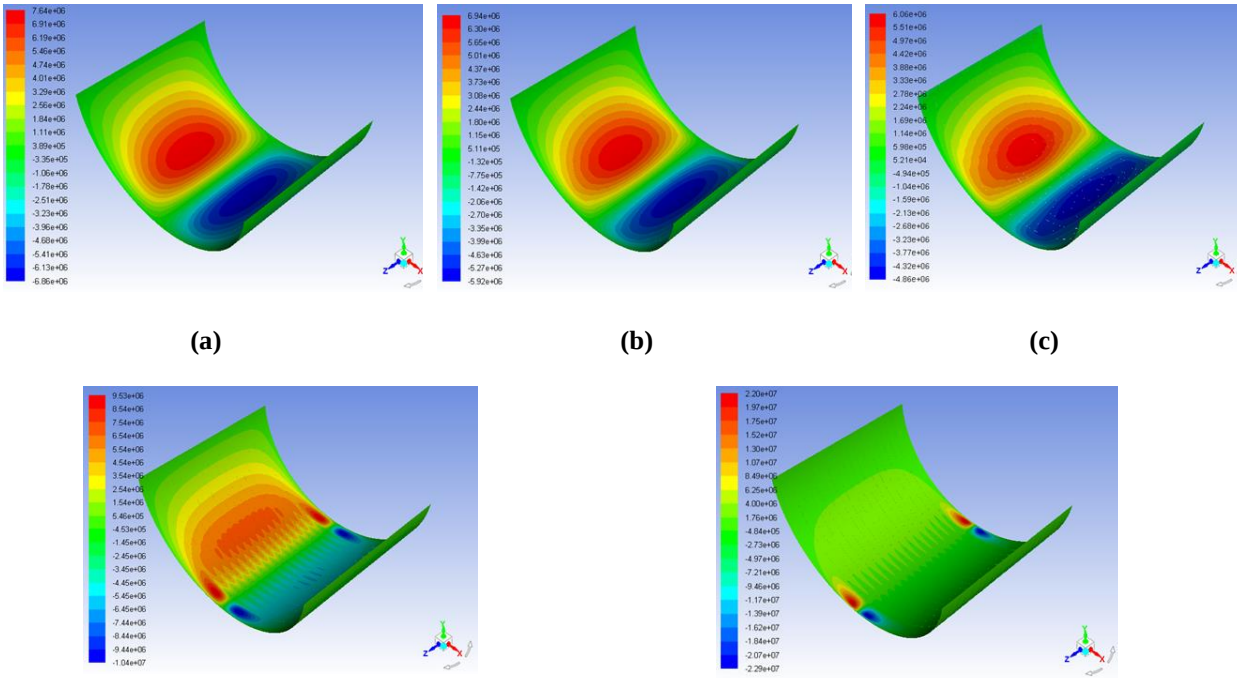

(a) **(b)** **(c)**

(d) **(e)**

Figure 9. Effect of scratch depth on thermo-hydrodynamic oil film pressure when arc bearing equal (170°) for L/D = 0.77, N=1500 r.p.m. (a)$h_s = 0C$(m) and $\varepsilon = 0.82$,(b) $h_s = 0.125C$(m) and $\varepsilon = 0.836$ (c) h_s =0.25C(m) and $\varepsilon = 0.8589$,(d) $h_s = 0.5C$(m) and $\varepsilon = 0.9616$ and (e) $h_s = C$(m) and $\varepsilon = 0.9866$.

Fig .10 shows the relation between scratch depth and thermo-hydrodynamic oil film pressure for both smooth and the scratch surface where the maximum static pressure found at the scratch depth equal to radial clearance ($h_s = C$).
Fig .11 shows the static oil film temperature for smooth and scratch surface where the maximum static temperature found at the scratch depth equal to radial clearance ($h_s = C$).
Fig. 12. shows the temperature distribution on oil film for arc bearing.

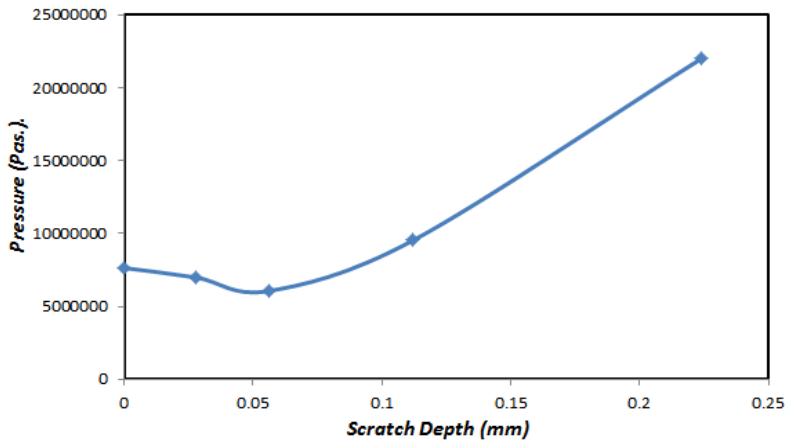

Figure 10. Thermo-hydrodynamic oil film pressure at various scratch depth when arc bearing equal (170°) for L/D=0.77 and N=1500 r.p.m.

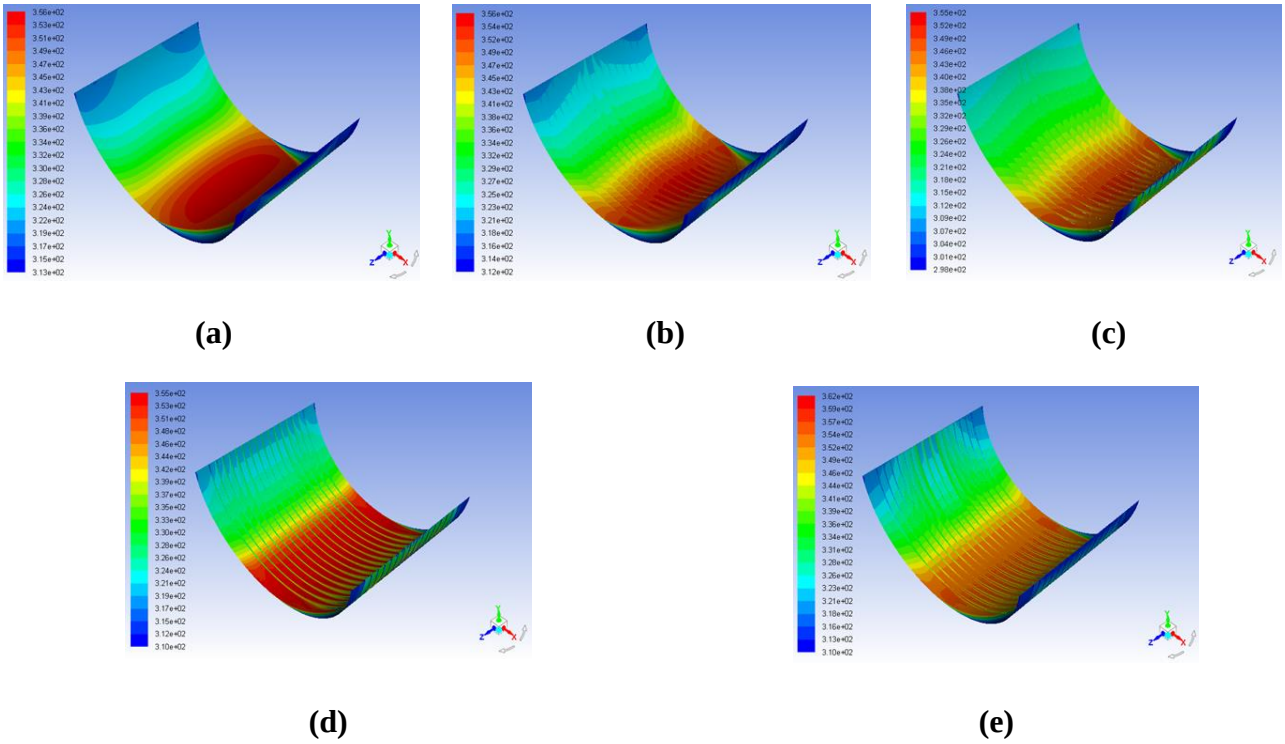

Figure 11. Effect of scratch depth on oil film temperature when arc bearing equal (170°) for L/D=0.77, N=1500 r.p.m. (a)$h_s = 0C$(m) and $\varepsilon = 0.82$,(b) $h_s = 0.125C$(m) and $\varepsilon = 0.836$, (c) h_s =0.25C(m) and $\varepsilon = 0.8589$,(d) $h_s = 0.5C(m)$ and $\varepsilon = 0.9616$and (e) $h_s = C$(m) and $\varepsilon = 0.9866$.

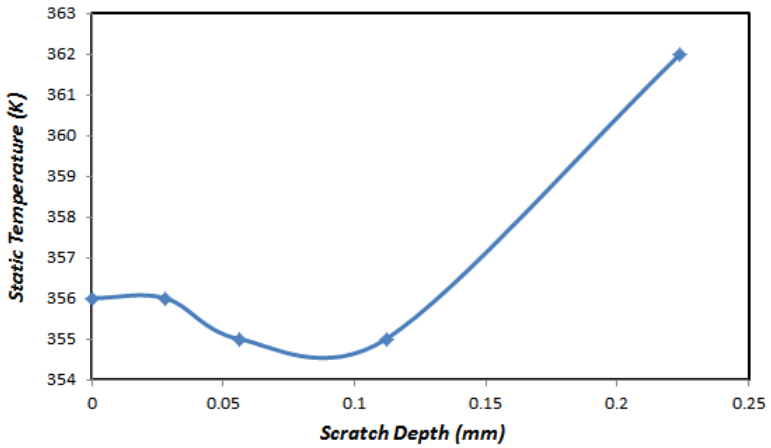

Figure 12. Temperature distribution on oil film for arc bearing equal (170°) for L/D=0.77 and N=1500 r. p. m.

As temperature levels rise due to heat generated by friction in the film layer, the solid bearing zone undergoes a thermal expansion varying locally according to the temperature gradients found at each spot of the bush. The bearing's inner surface is exposed to deformation due to the oil film

pressure and heat resulting from the friction between the fluid particles and the friction caused by the contact between the fluid surface and the solid surface (bearing) **Fig.13**.

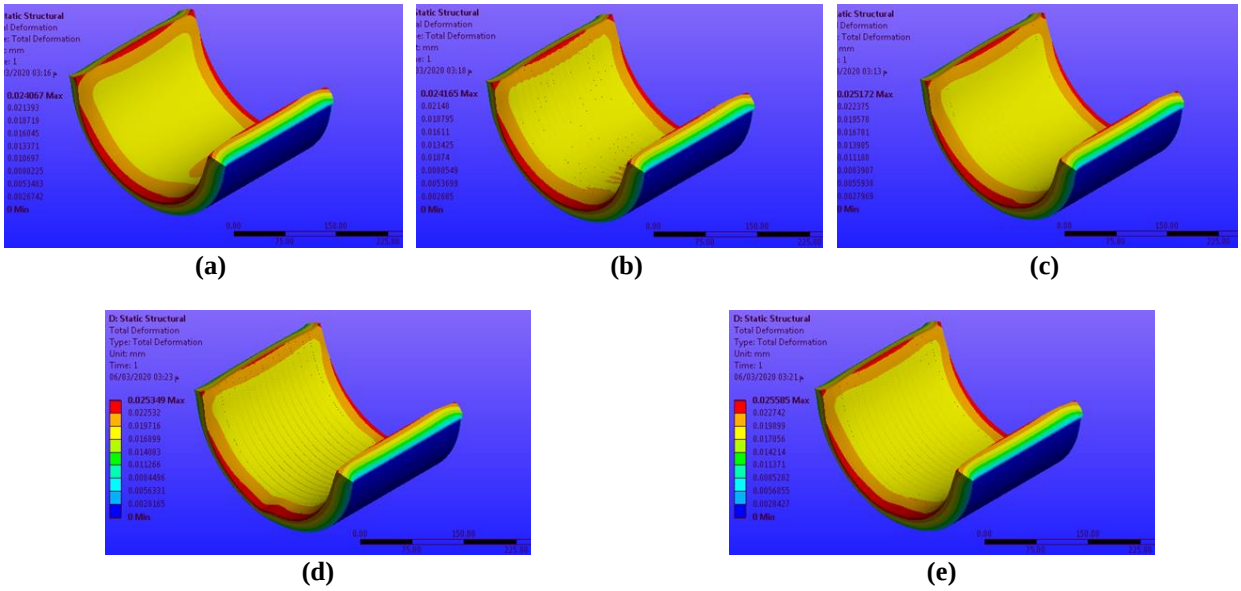

Figure 13. Effect of scratch depth on total deformation with the presence of an effect of temperature when arc bearing equal (170°) for L/D=0.77, N=1500 r.p.m. (a)$h_s = 0C$(m) and $\varepsilon = 0.82$,(b) $h_s = 0.125C$(m) and $\varepsilon = 0.836$,(c) h_s =0.25C(m) and $\varepsilon = 0.8589$,(d) $h_s = 0.5C$(m) and $\varepsilon = 0.9616$and (e) $h_s = C$(m) and $\varepsilon = 0.9866$.

Fig.14 shows the relation between scratch depth and total deformation for both smooth and the scratch surface where the maximum total deformation found at the scratch depth equal to radial clearance ($h_s = C$) .

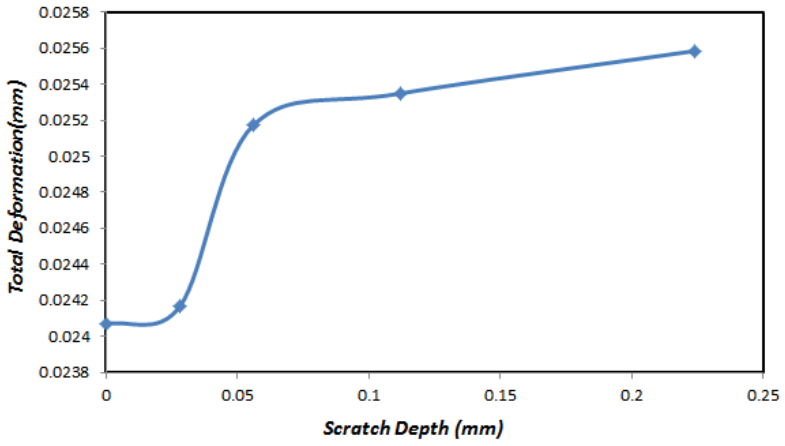

Figure 14. Total deformation on bearing shell at various scratch depth with the presence of an effect of temperature when arc bearing equal (170°) for L/D=0.77 and N=1500 r.p.m.

Due to that thermal deformation, the bearing is further stressed due to the temperature gradients generated. The wear deformation is always throughout the model. The occurrence of failure and was not taken into account, but the purpose is to calculate the stress only, as shown in **Fig. 15.**

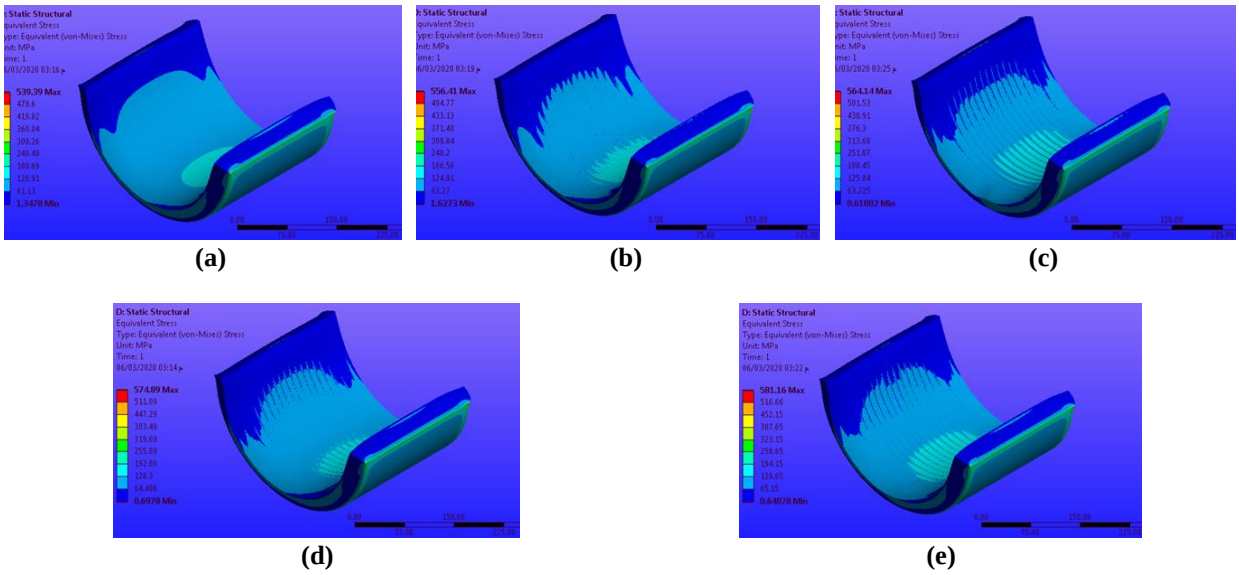

Figure 15. Effect of scratch depth on equivalent stress with the presence of an effect of temperature when arc bearing equal (170°) for L/D=0.77, N=1500 r.p.m. (a)$h_s = 0C(m)$ and $\varepsilon = 0.82$,(b) $h_s = 0.125C$(m) and $\varepsilon = 0.836$,(c) h_s =0.25C(m) and $\varepsilon = 0.8589$,(d) $h_s = 0.5C$(m) and $\varepsilon = 0.9616$ and (e) $h_s = C(m)$ and $\varepsilon = 0.9866$.

Fig. 16 shows the relation between scratch depth and equivalent stress for both smooth and the scratch surface where the maximum equivalent stress found at the scratch depth equal to radial clearance ($h_s = C$).

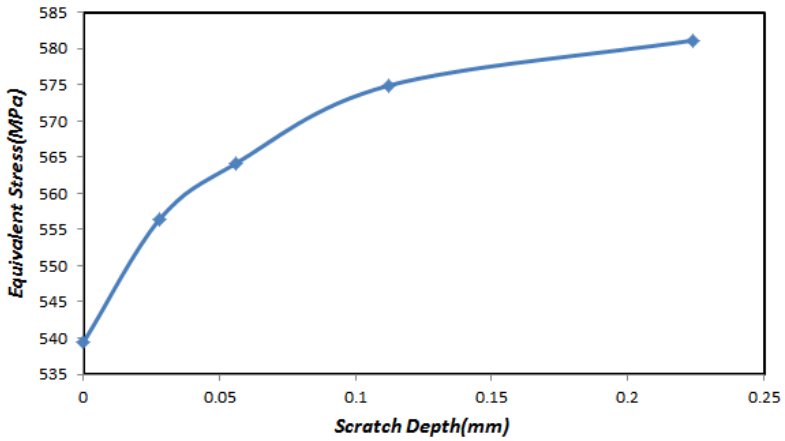

Figure 16. Equivalent stresses at various scratch depth with the presence of an effect of temperature when arc bearing equal (170°) for L/D=0.77 and N=1500 r.p.m.

5. CONCLUSIONS

The remarks concluded are as follows:

1- For a scratched journal bearing with a small scratch depth, i.e. $h_s = C/8$, the pressure is slightly affected. On the other hand, the performance is severely affected at deep scratches, i.e. $h_s = C$, where the bearing is likely subjected to complete damage due to severe mechanical and thermal loads concentrated on certain spots.

2- In scratched journal bearings, the maximum pressure developed in the oil is significantly affected by the extent of scratches depth. At a small depth of scratches, i.e. $h_s = C/8$, the pressure has been marginally affected compared to the deeper scratches, i.e. $h_s = C/2$, where the pressure is significantly increased. Similarly, the deepest scratches, i.e. $h_s = C$, result in severe effects on the pressure distribution on journal bearing surface where the pressure can be of destructive levels at certain spots.

3- The maximum deformation is generated at maximum pressure when the scratch depth equals the clearance value($h_s = C$).

4- The stresses are generated at maximum pressure when the scratch depth equals to the clearance value(h_s=C).

NOMENCLATURE

$\ddot{d}$ =Local acceleration of the solid region, m/s^2
e= journal eccentricity in bearing, m
f_s =Externally applied body force vector, N
FSI=Fluid Solid Interaction
h_{bo}= heat transfer coefficient on the outer bearing surface, W/m^2.$^\circ$C
O= bearing center, dimensionless
r = Radial position, m
T_{shaft}= shaft temperature, $^\circ$C
$\bar{T}_{shaft}$ = dimensionless shaft temperature, ^{o}C
T_o= Fresh oil(lubricant) temperature, ^{o}C
T_a= ambient temperature, ^{o}C
T_{bo}= outer bearing surface temperature, ^{o}C
UDF= User Define Function, dimensionless
U= Linear velocity, m/s
W= load applied, N

GREEK SYMBOLS

ε= eccentricity ratio, dimensionless
ω= rotational speed, rad/sec
γ= Recirculation Fraction, dimensionless
ρ_s =Solid density, kg/m^3
λ_s= bearing thermal conductivity, W/m. K
σ_s =Solid Cauchy stress tensor, Pa
β =Viscosity- temperature coefficient, dimensionless

SUBSCRIPTS

a = Ambinet
b_o= beraring outer surface
b_i= bearing inner surface

REFERENCES

- Abass, B. A., Hosain, A. M., and Sadiq, B. R, 2010. Surface Temperature Effect On The Thermohydrodynamic Performance Of Journal Bearing In Heavy Duty Machinery. *J. Eng.*, 16(4).pp. 6071-6084.
- Bhat, P., Shenoy, S., and Pai, R, 2007. Elastohydrodynamic Lubrication Analysis of a Radially Adjustable Partial Arc Bearing Using Fluid Structure Interaction. *Proc. ASME/STLE Int. Jt. Tribol. Conf.*, pp. 1–3.
- Dobrica, M. B., and Fillon, M., 2012. Performance degradation in scratched journal bearings. *Tribology International*. Elsevier, 51, pp.1- 10.
- Dobrica, M. B., Fillon, M., and Maspeyrot, P, 2006. Mixed Elastohydrodynamic lubrication in a partial journal bearing– comparison between deterministic and stochastic models. *Trans. ASME,* (128).pp. 1-12.
- Dobrica, M. B., Fillon, M., and Maspeyrot, P., 2008. Influence of mixed-lubrication and rough elastic-plastic contact on the performance of small fluid film bearings. *Tribol. Trans.*, 51(6) , pp.699- 717.
- Dobrica, M.B., and Fillon, M., 2008. Influence of scratches on the performance of a partial journal bearing. *ASME*, pp.1-3.
- Khonsari, M., and Booser, E. R., 2006. Effect of contamination on the performance of hydrodynamic bearings, J. Eng. Tribol., 220(5), pp. 419–428. DOI:10.1243/13506501J00705
- Liang, X. and Zhou., X. C.,2016. Hydrodynamic lubrication of partial textured sliding journal bearing based on three-dimensional CFD. *Ind. Lubr. Tribol.*, 68(1),pp. 106 - 115.
- Liu, H. *et al.*, 2010. Application of Computational Fluid Dynamics and Fluid-Structure Interaction Method to the Lubrication Study of a Rotor – Bearing System. *Tribology Letters*, (123), pp. 325-336. DOI: 10.1007/s11249-010-9612-6.
- Sharma, R.k., and Pandey, R.k., 2005. Effect of longitudinal surface roughness on the performance of thermohydrodynamically lubricated slider bearing-A Stochastic roughness Model, pp. 270-275. (Conference: 12th NaCoMM,16th -17th December At: IIT Guwahati, India).
- Vyas, P., 2005. Effects of stochastic (random) surface roughness on hydrodynamic lubrication of deterministic asperity.
- Versteeg, H. K., and Malalasekera, M., 2007. *An Introduction to Computational Fluid Dynamics: The Finite Volumes Method*. 2nd Edition, Essex: Pearson Education Limited.